# Dalton Transactions

Accepted Manuscript






ROYAL SOCIETY OF CHEMISTRY

www.rsc.org/dalton

Cite this: DOI: 10.1039/c0xx00000x

www.rsc.org/xxxxxx

ARTICLE TYPE

# Structure and temperature sensitive photoluminescence in a novel phosphate red phosphor $RbZnPO_4:Eu^{3+}$

**Shuangyu Xin, Yuhua Wang,* Ge Zhu, Xin Ding, Wanying Geng, Qian Wang**

***Received (in XXX, XXX) Xth XXXXXXXXX 20XX, Accepted Xth XXXXXXXXX 20XX***
**DOI: 10.1039/b000000x**

A novel phosphate $RbZnPO_4$ was firstly developed and characteristic crystal structure of $RbZnPO_4$ was investigated in detail, based on the Fourier transform infrared reflection spectra and the structure refinement of X-ray Diffraction data. After doping $Eu^{3+}$, $RbZnPO_4$: $Eu^{3+}$ shows distinctive deep red emission with dominated peaks at 596 and 701 nm. To provide a reasonable explanation for the relationship between photoluminescence and structure, the photoluminescence property is discussed by analyzing the especial local ligand environment and site occupying of $Eu^{3+}$ in $RbZnPO_4$. More interestingly, the temperature sensitive emission behavior was found in $RbZnPO_4:Eu^{3+}$. Through synthetically analyzing the configurational coordinate diagram, the charge compensation experiment and the CASTEP band structure calculation, a complex underlying mechanism is proposed to explain the abnormal temperature sensitive emission behavior in $RbZnPO_4:Eu^{3+}$. The mechanism could be helpful for better understanding the thermal quenching process of $Eu^{3+}$ in $RbZnPO_4$ and also in some other temperature sensitive phosphors as a reference.

## 1. Introduction

Trivalent Lanthanide ions ($Ln^{3+}$) doped materials are well-known due to their luminescent properties and have been utilized widely in display field and fluorescent lights in the past decades.[1] Among them, trivalent europium ($Eu^{3+}$) has played an important role as a luminescent ion due to its narrow emission bands mainly in the orange to red part of the visible spectrum, originating from internal $4f^6$-$4f^6$ electronic transitions.[2-4] Moreover, these transitions can be influenced by the local symmetry of $Eu^{3+}$, so $Eu^{3+}$ is widely used as a structure probe to investigate the crystallographic sites occupied by rare-earth ions in some new hosts.[5] The line emission of $Eu^{3+}$ is more suitable for display devices to provide highly color-pure red and nowadays, $Eu^{3+}$ doped $Y_2O_2S$ and $(Y,Gd)VO_4$ phosphors are used as commercial red phosphors with stable luminescent performances. However, they often suffer from low energy efficiency (lower than that of the blue phosphor $BaMgAl_{10}O_{17}:Eu^{2+}$ and green phosphor $ZnS:Cu^{+}$, $Al^{3+}$) at a given temperature and unstable chemical stability.[6,7] Therefore, it is urgent to search for a novel and highly efficient red phosphor, and more important is to figure out the energy transfer mechanics at elevated temperatures to better understand the emission quenching processes. At present, among the large number of photoluminescence material hosts available, phosphate compounds have attracted more and more attention for excellent thermal stability, good charge stability and low sintering temperature. Since early in 1962, phosphates with the general formula $ABPO_4$ (where A is a monovalent cation and B is a divalent cation) have been of interest for their optical or ferroelectric properties.[8,9] Recently, phosphors based on $ABPO_4$ have also been considered to be efficient luminescent hosts due to their excellent thermal and hydrolytic stability.[10,11] In 1969, Averbuch-Pouchot firstly reported a new phosphate $RbZnPO_4$ and in 1991, Elammari et al. reported the crystal structure of $RbZnPO_4$ (in French), but the report is not available online now.[12,13] Due to fundamental research and application demands, we systematically investigate a novel deep red emission phosphor $RbZnPO_4$: $Eu^{3+}$. The crystal structure is investigated through analyzing the Fourier transform infrared reflection spectra and the X-ray Diffraction structure refinement. The relationship between the characteristic photoluminescence property and the host structure is discussed in detail. Moreover, the temperature sensitive emission behavior is found in $RbZnPO_4:Eu^{3+}$ and an underlying mechanism is proposed to explain the abnormal temperature sensitive emission behavior based on the configurational coordinate diagram, the charge compensation experiment and the CASTEP (Cambridge Sequential Total Energy Package) band structure calculation.

## 2. Experimental

Samples of $Eu^{3+}$ doped $RbZnPO_4$ were synthesized by solid state reaction. Starting materials were $Rb_2CO_3$, ZnO, $(NH_4)_2HPO_4$, and $Eu_2O_3$ with a purity of 99.99 % and were supplied by Sinopharm Co., Ltd., China. The stoichiometric raw materials (Rb: Zn: P=1: 2: 2, the product amount was fixed at 1 gram) were ground thoroughly in an agate mortar for 1-2 h in alcohol. Subsequently, the dried power mixtures were fired in an alumina crucible and heated to 1073 K in air for 12 h. Then the preheated mixture was ground again and fired to 1373 K for 8 h in box-type furnace.

Finally the as-synthesized samples were slowly cooled down with a rate of 5 K/min to room temperature.

The crystal structure was identified by using a Rigaku D/Max-2400 X-ray diffractometer (XRD) with Ni-filtered Cu Kα radiation and Fourier transform infrared spectroscopy (FTIR, Nicolet NEXUS 670). The photoluminescence (PL) and PL excitation (PLE) spectra of the samples at room temperatures were measured by using an FL-1039 (Horiba Jobin Yvon) fluorescence spectrophotometer equipped with a 450 W xenon light source. The PL decay curves were measured by a FLS-920T fluorescence spectrophotometer with an nF900 ms Flashlamp as the light source. All of the measurements were performed at room temperature. High-temperature luminescence intensity measurements were carried out by using an aluminum plaque with cartridge heaters; the temperature was measured by thermocouples inside the plaque and controlled by a standard TAP-02 high-temperature fluorescence controller. The emission spectra and decay curves at low temperatures (form 10 K to 280 K) were measured by using FLS-920T fluorescence spectrophotometer under the protection of liquid nitrogen.

## 3. Results and Discussion

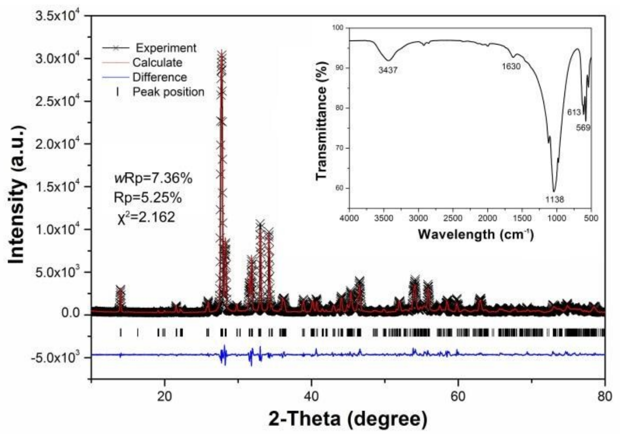


Figure 1 The experimental (crosses), calculated (solid line) and difference (bottom) results of XRD refinement of $RbZnPO_4$ host. The inset shows the FTIR spectrum of as-prepared $RbZnPO_4$ sample

The inset in Figure 1 shows the FTIR spectrum of as-prepared $RbZnPO_4$ host, which clearly displays several characteristic absorption bands of $PO_4^{3-}$ at 1138, 613 and 569 $cm^{-1}$.[14] The other two absorption bands at 3437 and 1630 $cm^{-1}$ can be attributed to OH vibrations (bending and stretching, respectively) of the adsorbed water on the surface of the phosphors. Figure 1 plots Rietveld structural refinements of powder diffraction patterns of $RbZnPO_4$ host at room temperature by General Structure Analysis System (GSAS).[15] The black short vertical lines show the position of Bragg reflections of the calculated pattern. The difference between the experimental and calculated patterns is plotted by blue line at the bottom. The structure parameters reported on $RbMnPO_4$ were used as initial parameters in the Rietveld analysis.[16] All the observed peaks satisfy the reflection condition and the final residual factors are also shown in Figure 1. The results indicate that the powder sample is crystallized in monoclinic symmetry with space group P121. The lattice parameters are a=8.8533 Å, b=5.4093 Å and c=8.9588 Å, respectively.

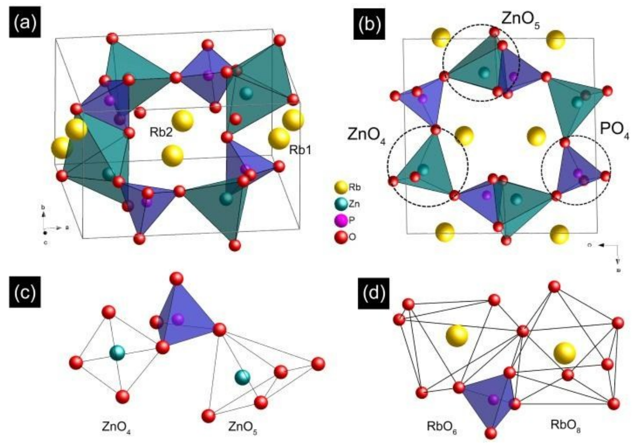


Figure 2 (a) The structural framework and coordination environments for all independent metal atoms in $RbZnPO_4$ view along [112] direction; (b) Structural views of $RbZnPO_4$ along [010] direction; (c) Partial projection of the structure of $RbZnPO_4$ with $ZnO_5/ZnO_4$ polyhedra. (d) Partial projection of the structure of $RbZnPO_4$ with $RbO_6$ and $RbO_8$ polyhedra. Green and blue polyhedral are $ZnO_5/ZnO_4$ and $PO_4$. Yellow spheres are $Rb^+$. Oxygen atoms at polyhedra vertices are not explicitly shown.

Figure 2a and 2b show the projections of the structures of $RbZnPO_4$ along [ 1 12] and [010] directions. All the bond distances and angles are in the normal range, and the detailed atomic coordinate information are given in Table 1 and the interatomic distances of Rb-O and Zn-O are shown in Table S1 of the supporting information. As shown in Figure 2a, the crystal structure of $RbZnPO_4$ is a three-dimensional framework consisting of $RbO_8/RbO_6$, $PO_4$ and $ZnO_5/ZnO_4$ polyhedra. In order to afford clear views of the structure, only $PO_4$ (blue part) and $ZnO_5/ZnO_4$ (green part) are presented as polyhedra in Figure 2a and 2b. The view from [112] direction clearly shows that the $ZnO_5/ZnO_4$ and $PO_4$ polyhedron form polyhedra rings around the a-axis to form layers which are interconnected and this stacking induces tunnels perpendicular to the a-axis with large cavities in which the Rb atoms are located, with six and eight coordinations. Figure 2c and 2d clearly show the coordination environment of Zn and Rb atoms in $RbZnPO_4$. The two different zinc positions of Zn1 and Zn2 are located in square-pyramid ($ZnO_5$) and tetrahedral ($ZnO_4$) coordination polyhedra, respectively. The Rb1 and Rb2 are also corner-sharing with $PO_4$ tetrahedron to form contorted octahedron and dodecahedron, as shown in Figure 2d. The effective ionic radii of the cations in $RbZnPO_4$ are listed in Table S2 in the supporting information.[17] Based on the effective ionic radius and the similar electric charge, when $Eu^{3+}$ enter into the lattice matrix, they are expected to randomly enter into $Zn^{2+}$ sites and experience specific local symmetry environment, that is, the non-centrosymmetrical Zn1 site and the centrosymmetrical Zn2 site. According to the Judd－Ofelt theory,[18] the electric dipole transition $^5D_0 \rightarrow {}^7F_2$ of $Eu^{3+}$ is hypersensitive, and the emission intensity is strongly influenced by ligand ions in the crystals. If $Eu^{3+}$ occupy an inversion symmetry site, a dominant reddish orange emission will be obtained according to the magnetic transition $^5D_0 \rightarrow {}^7F_1$. Conversely, an electric dipole transition $^5D_0 \rightarrow {}^7F_2$ with red emission will predominate in the

Cite this: DOI: 10.1039/c0xx00000x

www.rsc.org/xxxxxx

**ARTICLE TYPE**

emission spectra. It is interested that $Eu^{3+}$ may occupy both the two Zn sites with different local symmetry environments in $RbZnPO_4$. No report has been focused on such situation thus the photoluminescence property is of great anticipation.

Figure 3a shows the PLE spectra of $RbZnPO_4$:$x$$Eu^{3+}$ ($0.005 \le x \le 0.06$) monitored at 698 nm. It is clearly seen that the PLE spectra consists of a broad band centered at about 270 nm and several sharp peaks ranging from 300 to 500 nm. The former band excitation can be assigned to the charge transfer band (CTB), resulting from an electron transfer from the ligand $O^{2-}$

Table 1 The detailed atomic coordintes of $RbZnO_4$ according to the XRD refinement results

| Atom | Wyck. | x/a | y/b | z/c | Occu. | U [Å2] |
|---|---|---|---|---|---|---|
| Rb1 | 2a | 0.0079 | 0.2073 | 0.1943 | 1.00 | 0.0525 |
| Rb2 | 2a | 0.4974 | 0.6779 | 0.6933 | 1.00 | 0.0282 |
| Zn1 | 2a | 0.8262 | 0.7100 | 0.4229 | 1.00 | 0.0297 |
| Zn2 | 2a | 0.3299 | 0.6827 | 0.0894 | 1.00 | 0.0240 |
| P1 | 2a | 0.8072 | 0.2092 | 0.5810 | 1.00 | 0.0000 |
| P2 | 2a | 0.6863 | 0.6632 | 0.0970 | 1.00 | 0.0210 |
| O1 | 2a | 0.5325 | 0.7232 | 0.1746 | 1.00 | 0.0350 |
| O2 | 2a | 0.7936 | 0.7905 | 0.2091 | 1.00 | 0.0005 |
| O3 | 2a | 0.7444 | 0.3880 | 0.0514 | 1.00 | 0.0833 |
| O4 | 2a | 0.7285 | 0.8170 | -0.0329 | 1.00 | 0.1717 |
| O5 | 2a | 0.9808 | 0.2414 | 0.5002 | 1.00 | 0.1158 |
| O6 | 2a | 0.6566 | 0.9344 | 0.5325 | 1.00 | 0.1642 |
| O7 | 2a | 0.7570 | 0.4073 | 0.5093 | 1.00 | 0.0229 |
| O8 | 2a | 0.8037 | 0.2288 | 0.7367 | 1.00 | 0.0491 |

($2P^6$) orbital to the empty state of $4f^6$ in the $Eu^{3+}$ ion and the latter line peaks should related to the characteristic $4f$–$4f$ transitions of $Eu^{3+}$, as depicted in Figure 3a.[19] It should be noted that in the current phosphor $RbZnPO_4$:$Eu^{3+}$, the Eu-O CTB locates at short wavelength, which may have an effect on its thermal stability and will be discussed later. Figure 3b presents the PL emission spectra of $RbZnPO_4$:$x$$Eu^{3+}$ ($0.005 \le x \le 0.06$) phosphors excited at 393 nm. The spectra consist of a number of sharp lines ranging from 500 to 750 nm, which are associated with the transitions from the excited state $^5D_{0,1}$ to $^7F_J$ (J=0, 1, 2, 3, 4) levels of $Eu^{3+}$.[19] The small emission peak at 580 nm is attributed to $^5D_0 \rightarrow {}^7F_0$ transition. The peaks around 590 and 612 nm are resulted from the magnetic dipole transition $^5D_0 \rightarrow {}^7F_1$ and the electric dipole transition $^5D_0 \rightarrow {}^7F_2$, respectively. The weak emission located at 647 nm is due to the $^5D_0 \rightarrow {}^7F_3$ transition and the multi-emissions with main components peaking at 680, 691 and 701 nm are caused by the $^5D_0 \rightarrow {}^7F_4$ transition. The line shape of emission does not change with the variation of $Eu^{3+}$ concentrations. Because most of the valence electrons of trivalent rare-earth elements are shielded by 5s and 5p outer electrons, and f-f transitions of trivalent lanthanides are weakly affected by ligand ions in the crystals. However, a few transitions of the trivalent lanthanides are sensitive to the environment of the crystal, and these have been called hypersensitive transitions.[20] As mentioned above, the electric dipole transition $^5D_0 \rightarrow {}^7F_2$ of $Eu^{3+}$ is hypersensitive and can be used as a probe to detect the occupying situation of $Eu^{3+}$ in a host. The intensity ratio of $^5D_0 \rightarrow {}^7F_2$ to $^5D_0 \rightarrow {}^7F_1$ is usually regarded as a measure of site symmetry around the $Eu^{3+}$. In this case, the dominated orange emission at 594 nm is attributed to the magnetic transition $^5D_0 \rightarrow {}^7F_1$, and the ratio of $^5D_0 \rightarrow {}^7F_2$ to $^5D_0 \rightarrow {}^7F_1$ transitions is 0.68, which is quite smaller than that of common red phosphors, typically $Y_2O_3$:$Eu^{3+}$ (3.8), and is closed to that in $YPO_4$: $Eu^{3+}$ (0.978), $GdPO_4$:$Eu^{3+}$ (0.715). [21-23] The ratio of $^5D_0 \rightarrow {}^7F_2$ to $^5D_0 \rightarrow {}^7F_1$ transitions indicates that the local symmetry around most $Eu^{3+}$ is centrosymmetric, indicating that most $Eu^{3+}$ are more inclined to occupy the Zn2 sites with tetrahedral coordination. However, we think there are still some $Eu^{3+}$ occupy the Zn1 sites with five oxygen coordinations because the abnormal higher intensity of the $^5D_0 \rightarrow {}^7F_4$ transition at 699 nm is also observed and as strong as the $^5D_0 \rightarrow {}^7F_1$ transition. Generally, the abnormal phenomenon may due to the distortion of $Eu^{3+}$ local symmetry group, and the electronegativity and ionic radius of cations in a matrix structure.[21,22] Thus, the reason of the observed unusual strong transition of $^5D_0 \rightarrow {}^7F_4$ is complicated; however, it is clear that it should be related to the environment around $Eu^{3+}$ because there are diverse contorted polyhedra, such as $RbO_6$, $RbO_8$ and $ZnO_5$ and when $Eu^{3+}$ occupy Zn2 sites, the $^5D_0 \rightarrow {}^7F_4$ transition will be strong due to the disordered local environment.[16, 24-26]

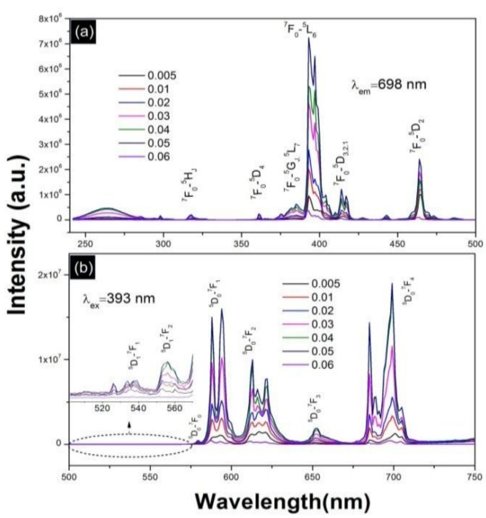


Figure 3 (a) The PLE spectra of $RbZnPO_4$:$x$$Eu^{3+}$ ($0.005 \le x \le 0.06$) monitored at 698 nm; (b) the PL emission spectra of $RbZnPO_4$:$x$$Eu^{3+}$ ($0.005 \le x \le 0.06$). Inset shows the magnified transitions from upper energy levels of $Eu^{3+}$ in $RbZnPO_4$ host.

Some rare weak emissions from upper level $^5D_1$ of $Eu^{3+}$ are shown in the magnified inset of Figure 3b. According to the related reports, it is related to the multiphonon relaxation process of $Eu^{3+}$ in different matrix structure.[27,28] The nonradiative transitions rate between levels of a $4f^n$ configuration of rare-earth ions is given by[29]

$$W_{nR} = W_{nR}(0)\exp(-\alpha n\hbar\omega_p)$$

Where α depends on the electron-phonon interaction, $W_{nR}$ is the relaxation rate, $\hbar\omega_p$ is the highest available vibrational phonon energy. $n = \Delta E / \hbar\omega_p$ is the number of phonons to fill the energy gap and ΔE is the energy difference between the levels. The presence of emission lines from higher excited state $^5D_1$ is attributed to the low vibration energy $\hbar\omega_p$ of $(PO_4)^{3-}$ groups. The vibration energy of the $(PO_4)^{3-}$ groups in $RbZnO_4$ structure is around 500~1100 $cm^{-1}$ according to the FTIR results in the inset of Figure 1. The multiphonon relaxation by $(PO_4)^{3-}$ is not enough to bridge the gaps between the higher energy levels $^5D_1$ and $^5D_0$, resulting in weak emissions from these levels. To investigate the concentration dependent luminescence properties of $Eu^{3+}$ doped host, the luminescence properties of $RbZnO_4$: $x$$Eu^{3+}$ ($0.005 \leq x \leq 0.06$) samples were measured as shown in Figure 3b. With the increase of $Eu^{3+}$, the intensity of $Eu^{3+}$ emission increases rapidly and reaches a maximum at $x$=0.05 and then remarkably decreases when $Eu^{3+}$ content is further increased due to the concentration quenching effect, that is, when the $Eu^{3+}$ content increases, more and more $Eu^{3+}$ pair or aggregate with others, efficient resonant energy transfers between $Eu^{3+}$ and a fraction of $Eu^{3+}$ migrates to distant luminescent killer, leading to the luminescence quenching. The quantum efficiency of $RbZnPO_4$:$0.05Eu^{3+}$ phosphor was also measured to be 41.6% through the integrating sphere method.

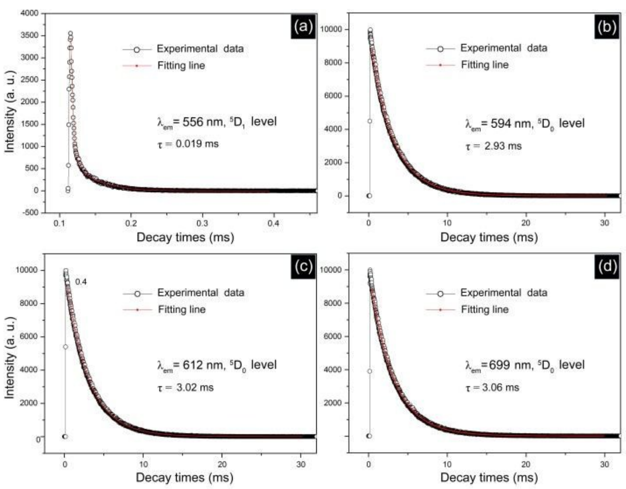


Figure 4 The decay curves of $RbZnO_4$:$0.05Eu^{3+}$ phosphor excited at 393 nm and monitored at (a) 556 nm, (b) 594 nm, (c) 612 nm and (d) 699 nm.

Figure 4a-4d shows the luminescence decay curves of $RbZnO_4$:$0.05Eu^{3+}$ phosphor excited at 393 nm. All the curves can be well fitted by exponential function and the lifetime value can be given to the average lifetime defined as: [19,30]

$$\tau_{average} = \frac{\int tI(t)dt}{\int I(t)dt}$$

Generally, the higher energy level is more metastable than the lower energy level, and the electron at the higher energy level would like to either transition to the ground ($^7F_J$, J=1,2,3,4) state or relax to the low energy level nonradiatively by multiphonon emission.[31] As a result, luminescence decay curves can also be used to distinguish the lower level $^5D_0$ with upper levels, such as $^5D_1$, $^5D_2$ or $^5D_3$ of $Eu^{3+}$. According to the fitting data, the lifetimes of the emission at 592 nm ($^5D_0 \rightarrow {}^7F_1$), 612 nm ($^5D_0 \rightarrow {}^7F_2$) and 699 nm ($^5D_0 \rightarrow {}^7F_4$) are calculated to be 2.93, 3.02, 3.06 ms, respectively (Figure 4b-d). There is almost no difference between the lifetimes of the above three emissions because they are all derived from the same energy level $^5D_0$. However, the lifetime of the emission at 556 nm ($^5D_1 \rightarrow {}^7F_2$) is calculated to be 0.019 ms (Figure 4a), which is much shorter than those of $^5D_0$ energy levels. The lifetimes of $Eu^{3+}$ in the current host are short enough for application in displays and lighting.

A comprehensive understanding of the thermal quenching mechanism in phosphors is indispensable because many devices suffer from thermal problems, whether they are applied in solid state lighting or in temperature sensing. Till now, numerous investigations about the thermal quenching property in phosphors have been discussed and the thermal quenching behavior can be resumptively summarized as the following rules: (a) increases with increasing energy separation of the ground and excited state; (b) increases with increasing phonon frequencies (thus most organic compounds exhibit luminescence only at low temperatures); (c) increases with $\Delta r = r_e - r_g$; where r means the average distance between the low point of the excited state and the ground state; (d) thermal quenching due to photoionization concerns luminescent materials, where the excited state is located close to the conduction band.[32] Generally, for the distance Δr for trivalent rare earth ions with f-f transitions, such as $Eu^{3+}$, is approximately equal to 0, which leads to the higher energy barrier from the excited states to ground state, and further results in the better thermal stability. Figure 5a shows the temperature dependent emission spectra of $RbZnPO_4$:$0.05Eu^{3+}$. The result indicates that $RbZnPO_4$:$0.05Eu^{3+}$ shows extraordinarily temperature sensitive emission and the relative emission intensity has dropped by a factor of 90 % from the initial intensity at 230 ℃. The unexpected result is interesting and it is significant to find out the mechanism for the temperature sensitive thermal quenching process of $Eu^{3+}$ in $RbZnPO_4$. Numbers of works discussed the thermal quenching process of $Eu^{3+}$ through a crossover from the $^5D_0$ excited state to the CTB because in these cases the Eu-O CTB locates at longer wavelength (above 300 nm) and such located $O^{2-}$ to $Eu^{3+}$ CTB can provide a path to relaxation of the excited state via a nonradiative process.[33,34] The crossover process can be described by the an Arrhenius-type activation model as[35]

$$I(t) = I_0[1 + A\exp(-\frac{\Delta E}{kT})]^{-1}$$

where $I$ is the intensity at a given temperature, $I_0$ is the initial intensity, k is the Boltzmann's constant, T is temperature, and ΔE

Cite this: DOI: 10.1039/c0xx00000x

www.rsc.org/xxxxxx

**ARTICLE TYPE**

is the activation energy from the $^5D_0$ state to the CTB and can be regarded as a constant because the shape of the emission curve did not change significantly. As displayed in Figure 5b, the experimental data can be fitted by a linear fit, indicating that the temperature quenching process complies well with the Arrhenius-

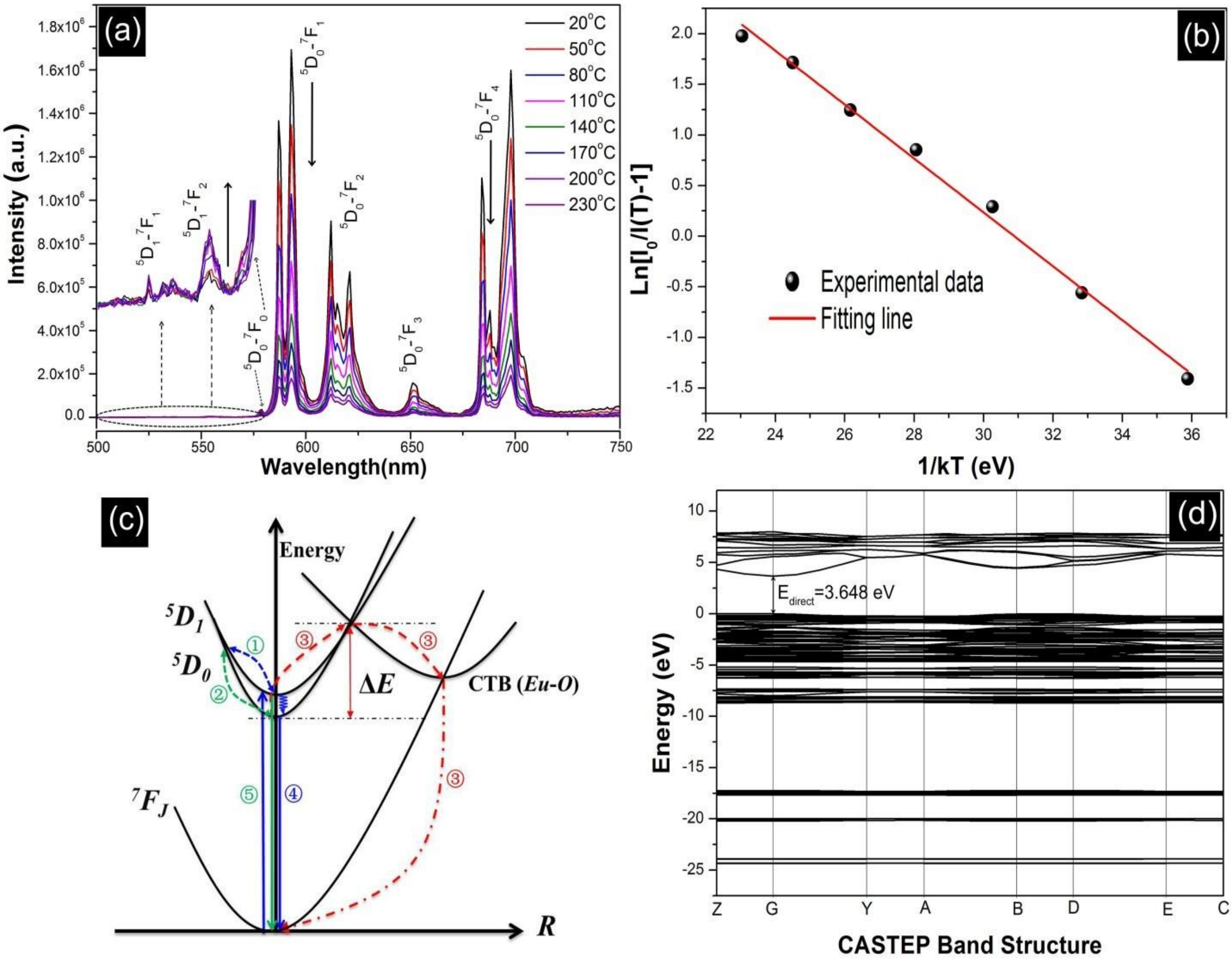


Figure 5 (a) The temperature dependent emission spectra of $RbZnO_4$:0.05$Eu^{3+}$ phosphor. The magnifying part reveals the usual thermal properties of the emission from higher $^5D_1$ energy; (b) the calculated activation energy for thermal quenching of $RbZnO_4$:0.05$Eu^{3+}$ phosphor; (c) Schematic illustration of a configurational coordinate diagram of the thermal quenching process and abnormal thermal luminescence property in $RbZnO_4$:0.05$Eu^{3+}$; (d) the calculated CASTEP band structure based on density functional theory.

type activation model. The activation energy of $RbZnPO_4$:0.05$Eu^{3+}$ phosphor is calculated to be 0.31 eV, which is much larger than those of $Eu^{3+}$ reported in other works. It is interesting but reasonable because it can be seen from Figure 2a that in $RbZnPO_4$:0.05$Eu^{3+}$, the $O^{2-}$ to $Eu^{3+}$ CTB locates at much shorter wavelength (~260 nm), which results in a large energy difference between the Eu-O CTB and the $^5D_0$ energy level, as depicted in the configurational coordination diagram as shown in Figure 5c . Generally, the $^5D_1$ is relaxed by cross-relaxation to the $^5D_0$ state (via pathway ①) and then some electrons can overcome the activation energy assisted by phonons as the temperature increases through the pathway ③ ($Eu^{3+}$-$O^{2-}$ CTB) and feed to the $^7F_J$ state, providing the nonradiative process, and the remaining electrons are contributed to the $^5D_0 \rightarrow ^7F_J$ emission (via pathway ④ ). However, the Arrhenius-type activation model can reasonably interpret one of the thermal quenching paths of $Eu^{3+}$ but cannot explain why it is so temperature sensitive in the current host $RbZnPO_4$. It should be noted that due to the large activation energy value of ΔE in $RbZnPO_4$:0.05$Eu^{3+}$, it is difficult for all the electrons return to the ground state through a crossover from the $^5D_0$ excited state to the CTB. Thus, other paths must be taken into account to interpret the temperature sensitive emission spectra. Firstly, the charge compensation mechanism is proposed for the current host. When trivalent $Eu^{3+}$ are doped into $RbZnPO_4$, they would non-equivalently replace the $Zn^{2+}$. In order to keep the charge balance, two $Eu^{3+}$ would be needed to substitute for three $Zn^{2+}$ (the total charge of two trivalent $Eu^{3+}$ is equal to that of three $Zn^{2+}$) and generate one vacancy defect of $V_{Zn}''$ with two negative charges, and two positive defects of $Eu_{Zn}^{\cdot}$ would be created by each substitution of every two $Eu^{3+}$ in the compound. The vacancy $V_{Zn}''$ would act as a “kill center”, which means impurity trapped excitation state and some electrons may enter in to these “kill centers” under the thermal stimulation, causing the temperature quenching process.[36] To verify this viewpoint, a common charge compensation agent $Li_2CO_3$ is added to $RbZnPO_4$:$0.05Eu^{3+}$ and the thermal quenching property is also shown in the Figure S1 of the supporting information. It is clear that the thermal quenching property decreases after doping the charge compensation agent $Li_2CO_3$, indicating that the charge compensation experiment is available in the thermal quenching process of $Eu^{3+}$ in $RbZnPO_4$. Secondly, thermally activated ions photoionization process should be considered. In some other temperature sensitive phosphors, the thermally activated ions photoionization also plays an important effect on the thermal quenching process.[36-38] Generally, the photoionization is complicated and it is difficult to find the direct evidence to prove it in the current host. In this work, the density functional theory calculations of $RbZnPO_4$ based on refined crystal structure data are performed and the CASTEP band structure is shown in Figure 5d. The local density approximation (LDA) was chosen as the theoretical basis of the density function. The result shows that this compound possesses a direct band gap of 3.648 eV with the valence band (VB) maximum and the conduction band (CB) minimum at G point of the Brillouin zone. Due to the direct band gap with such narrow band gap value, some electrons on the excited state may enter into the conduction band under the thermal stimulated effect and also promote the temperature sensitive thermal quenching process in $RbZnPO_4$:$0.05Eu^{3+}$. Apart from the temperature sensitive emission spectra, another interesting phenomenon also draws our attention, that is, the emission intensity of $^5D_1$ was found to increase gradually with increasing the temperature, which is contrary to that of $^5D_0$ energy level. The unusual $^5D_1$ emission can be explained as following: under the thermal stimulation effect, the electrons are activated from $^5D_0$ state to cross the point of intersection of the $^5D_1$ and $^5D_0$ curves (from ② to ①); then the $^5D_1 \rightarrow {}^7F_J$ at 556 nm is promoted via ⑤. Similar phenomenon has also been discussed in our previous work.[39] In addition, as shown in Figure S1, the thermal quenching behavior appears linear change from room temperature to 110 °C, indicating that it may have potential to be used in luminescence-based thermometer.[40]

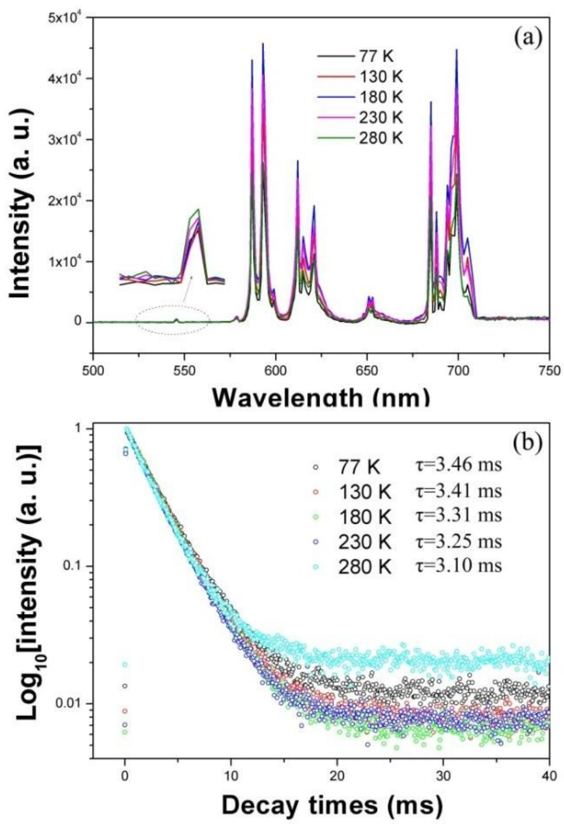


Figure 6 (a) The temperature dependent emission spectra measured from 10 K to 280 K; (b) the decay times of $^5D_2$ energy level under different temperatures.

Additionally, in order to further investigate the unusual thermal behaviour, the luminescence property at low temperature from 77 K to 280 K was measured, as illustrated in Figure 6a. As increasing the temperature, the emission intensity of the upper energy level $^5D_1$ was found to be tardily increased while that of $^5D_0$ energy level was found to be decreased, which showed similar property with the emission spectra measured at high temperature and indicated that the unusual behaviour as discussed in Figure 5c also took effect at low temperature. The decay times of $^5D_2$ energy level was measured excited at 393 nm and monitored at 612 nm. The decay curves can be well fitted by exponential function and the lifetime values were calculated to be 3.46, 3.41, 3.31, 3.25 and 3.10 ms, respectively. The decreased decay times can be attributed to increased interaction between $Eu^{3+}$ ions when rising the temperature.

## 4. Conclusions

In summary, a novel phosphate phosphor $RbZnPO_4$: $Eu^{3+}$ was developed and the crystal structure was investigated based on the FT-IR spectrum and XRD structure refinement. The abnormal photoluminescence properties of $RbZnPO_4$: $Eu^{3+}$ were studied and the relationship between the structure and the characteristic emission of $Eu^{3+}$ in $RbZnPO_4$ were provided. Under 393 nm excitation, $RbZnPO_4$: $Eu^{3+}$ showed red emission peaking at 594, 612 and 699 nm, corresponding to the $^5D_0$ to $^7F_J$ (J=1, 2, 4) transitions of $Eu^{3+}$ occupying both of the centrosymmetric Zn1 and the non-centrosymmetrical Zn2 sites. Upon the thermal stimulus, $RbZnPO_4$: $Eu^{3+}$ exhibited unusual temperature sensitive emission spectra. The underlying mechanisms were proposed and proved to explain the temperature sensitive emission behavior, by using the Arrhenius-type model in the configurational coordinate diagram, the charge compensation experiment and the CASTEP band structure calculation.

## Acknowledgements

This work is supported by the Specialized Research Fund for the Doctoral Program of Higher Education (no. 20120211130003), the National Natural Science Funds of China (Grant no. 51372105) and the Fundamental Research Funds for the Central Universities (No. lzujbky-2014-231). Thanks for the support of Gansu Province Development and Reform Commission and Ministry of Industry and Information Technology of the Gansu Province.

## Notes and references

*Department of Materials Science, School of Physical Science and Technology, Lanzhou University, Lanzhou, 730000, PR China and Key Laboratory for Special Function Materials and Structural Design of the Ministry of Education, Lanzhou University, Lanzhou 730000, China. Fax: +86-931-8913554; Tel: +86-931-8912772; E-mail: wyh@lzu.edu.cn*

† Electronic Supplementary Information (ESI) available. See DOI: 10.1039/b000000x/

## References

1. Z. Wang, Y. Li, Q. Jiang, H. Zeng, Z. Ci and L. Sun, *J. Mater. Chem. C*, 2014, **2**, 4495.
2. G. L. Law, W. M. Kwok and W. T. Wong, *J. Phys. Chem. B*, 2007, **111**, 10858.
3. W. S. Lo, W. M. Kwok, G. L. Law, C. T. Yeung, C. T. L. Chan, H. L. Yeung, H. K. Kong , C. H. Chen, M. B. Murphy, K. L. Wong and W. T. Wong, *Inorg. Chem.*, 2011, **50**, 5309.
4. J. W. Walton, R. Carr, N. H. Evans, A. M. Funk, A. M. K, D. Parker , D. S. Yufit, M. Botta, S. D. Pinto and K. L. Wong, *Inorg. Chem.*, 2012, **51**, 8042.
5. V. A. Morozov, A. Bertha, K. W. Meert, S. V. Rompaey, D.Batuk, G. T. Martinez, S. V. Aert, P. F. Smet, M.V. Raskina, D. Poelman, A. M. Abakumo and J. Hadermann, *Chem. Mater*., 2013, **25**, 4387.
6. Y. Huang, X. Wang, H. Lee, E. Cho, K. Jang and Y. Tao, *Phys. D: Appl. Phys.*, 2007, **40**, 7821.
7. P. Pust, V. Weiler, C. Hecht, A. Tücks, A. S. Wochnik, A. Hen, D. Wiechert, C. Scheu, P. J. Schmidt, W. Schnick, *Nat. Mater*. 2014, **13**, 891.
8. D. Blum, J. Penzin and J. Henry, *Ferroelectric*, 1984, **61**, 265.
9. C. Lin, Z. Xiao, G. Guo, T. Chan and R. Liu, *J. Am.Chem. Soc.*, 2010, **132**, 3020.
10. S. Zhang, Y. Nakai, T. Tsuboi, Y. Huang and H. Seo, *Chem. Mater.*, 2011, **23**, 1216.
11. M. A. Pouchot，*Mat. Res. Bull.*, 1969, **4**, 851. (in French)
12. L. Elammari and B. Elouadi, *Journal de chimie physique*, 1991, **88**, 1969. (in French)
13. L. Popović, D. Waal and J. Boeyens, *J. Raman Spectrosc*., 2005, **36**, 2.
14. A. Larson and R. Dreele, *General Structure Analysis System (GSAS)*, Technical Report for the Los Alamos National Laboratory, Los Alamos, 2004.
15. H. Yahia, E. Gaudin and J. Darriet, *J. Alloys Compd.*, 2007, **442**, 74.
16. R. Shannon, *Acta Cryst.*, 1976, **32**, 751.
17. N. Yamashita, *J. Phys. Soc. Jpn.*, 1973, **35**, 1089.
18. F. Du, Y. Nakai, T. Tsuboi, Y. Huang and H. Seo, *J. Mater. Chem.*, 2011, **21**, 4669.
19. S. Ye, F. Xiao, Y. Pan, Y. Y. Ma and Q. Zhang, *Mater. Sci. Eng., R*, 2010, **71**, 1.
20. H. Song, B. Chen, B. Sun, J. Zhang and S. Lu, *Chem. Phys. Lett.*, 2003, **372**, 368.
21. U. Rambabu and S. Buddhudu, *Opt. Mater.*, 2001, **17**, 401.
22. L. Yu, D. Li, M. Yue, J. Yao and S. Lu, *Chem. Phys.*, 2006, **326**, 478.
23. R. Skaudzius, A. Katelnikovas, D. Enseling, A. Kareiva and T. Jüstel, *J. Lumin.*, 2014, **147**, 290.
24. J. Wang, Y. Cheng, Y. Huang, P. Cai, S. Kim and H. Seo, *J. Mater. Chem. C*, 2014, **2**, 5559.
25. R. Ferreira, S. Nobre, C. Granadeiro, H. Nogueira, L. Carlos and O. Malta, *J. Lumin.*, 2006, **121**, 561.
26. X. Liu, C. Li, Z. Quan, Z. Cheng and J. Lin, *J. Phys. Chem. C*, 2007, **111**, 16601.
27. Y. Chang, C. Liang, S. Yan and Y. Chang, *J. Phys. Chem. C*, 2010, **114**, 3645.
28. S. Shionoya and W. Yen, *Phosphor Handbook*, CRC Press, Boca Raton, 1999.
29. Y. Tian, B. Chen, R. Hua, J. Sun, L. Cheng, H. Zhong, X. Li, J. Zhang, Y. Zheng, T. Yu, L. Huang and H. Yu, *J. Appl. Phys.*, 2011, **109**, 053511.
30. X. Liu, C. Li, Z. Quan, Z. Cheng and J. Lin, *J. Phys. Chem. C*, 2007, **111**, 16601.
31. D. Bertram, M. Born and T. Jüstel, *Springer Handbook of Lasers and Optics*, Springer Science, New York, 2007.
32. Y. Chang, C. Liang, S. Yan and Y. Chang, *J. Phys. Chem. C*, 2010, **114**, 3645.
33. Y. Fang, S. Chu, P. Kao, Y. Chuang and Z. Zeng, *J. Electrochem. Soc.*, 2011, **158**, 1.
34. B. Tian, B. Chen, Y. Tian, X. Li, J. Zhang, J. Sun, H. Zhong, L. Cheng, S. Fu, H. Zhong, Y. Wang, X. Zhang, H. Xia and R. Hua, *J. Mater. Chem. C*, 2013, **1**, 2338.
35. Z. Xia, L. Liao, M. Xiong and G. Li, *J. Lumin.*, 2013, **134**, 227.
36. C. R. Ronda, L. E. Shea, A. M. Srivastava, Physics and Chemistry of Luminescent Materials, The Electrochemical Society, 2000;
37. A. Setlur and U. Happek, *ECS Trans.*, 2009, **16**, 51.
38. G. Zhu, Z. Ci, Y. Shi, M. Que, Q. Wang and Y. Wang, *J. Mater. Chem. C*, 2013, **1**, 5960.
39. X. He and B. Yan, *CrystEngComm*, 2015, **17**, 62.
40. J. Dong and J. Zink, *ACS Nano*, 2014, **8**, 5199.

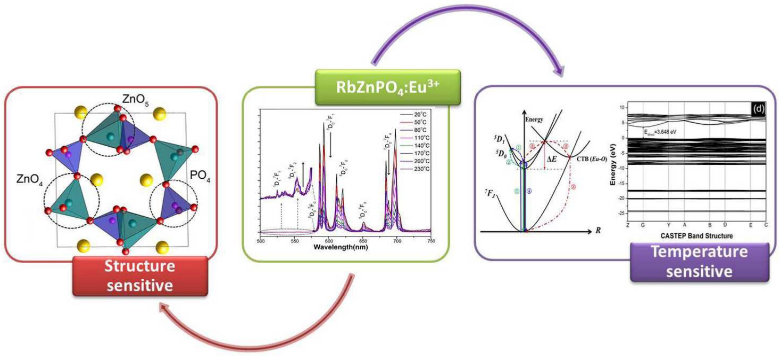


Colour graphic

Text:

Synthesis, crystal structure and temperature sensitive photoluminescence of a novel red phosphor $RbZnPO_4:Eu^{3+}$.

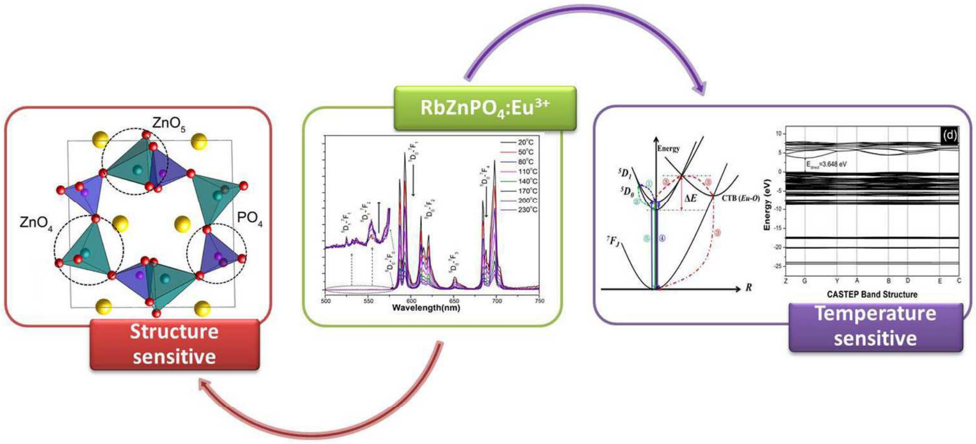


The luminescence properties investigation of a structure and temperature sensitive red phosphor RbZnPO4:Eu3+
254x129mm (300 x 300 DPI)